

## Peripherality and exchange mechanisms of four-body final states induced by $\pi^+p$ and $\bar{p}p$ interactions\*

D. Bastien, B. Haber,<sup>†</sup> M. F. Hodous, R. I. Hulsizer, V. Kistiakowsky,  
I. A. Pless, R. A. Singer, J. Wolfson, and R. K. Yamamoto  
*Massachusetts Institute of Technology, Cambridge, Massachusetts 02139*

P. Bastien, L. Kirkpatrick, and H. J. Lubatti<sup>‡</sup>  
*University of Washington, Seattle, Washington 98103*

(Received 13 September 1973)

We define a kinematical variable  $P_v$  which is correlated to the peripherality of a multibody final state.  $P_v = 0$  implies that all the final-state particles lie in a plane perpendicular to the incident direction.  $P_v = 1$  implies that all the particles in the final state are collinear with the incident direction.  $P_v$  distributions for resonance production are quite different from those for Lorentz-invariant phase space. This property may be used to detect phase-space-like phenomena at high energies in multibody final states ( $n \geq 10$ ). We compare  $P_v$  distributions for the four-body annihilation and nonannihilation channels of  $\bar{p}p$  interactions and the four-body final states of  $\pi^+p$  interactions in which the proton goes into the backward and forward hemispheres. We find remarkable kinematic similarities between annihilation and  $\pi^+p$  backward-hemisphere channels. We suggest that this is due to the dominance of baryon exchange. There is also a remarkable, but different, similarity between nonannihilation and the  $\pi^+p$  forward-hemisphere channels. We suggest that this is due to the dominance of meson exchange.

### I. INTRODUCTION

In this paper we define a kinematical peripherality variable  $P_v$  which is related to the peripherality of a multibodied final state. It takes on values  $0 \leq P_v \leq 1$ . When  $P_v = 1$ , then all the particles in the final state are collinear with the incident direction.  $P_v = 0$  implies that all final-state particles lie in a plane perpendicular to the incident direction. In Sec. II we define  $P_v$  and indicate its relationship to the Feynman  $X$  variable. In Sec. III we describe the properties of  $P_v$ . We compare the distribution of  $P_v$  corresponding to the assumption that the final-state particle correlations conform to Lorentz-invariant phase space with that for the assumption of resonant production and decay in the final state. We demonstrate that the distribution of the variable  $P_v$  has markedly different characteristics for these two assumptions. In Sec. IV we apply this variable to the study of four-body  $\bar{p}p$  and  $\pi^+p$  induced final states. We find that four-pion  $\bar{p}p$  annihilation events and  $\pi^+p$  induced backward two-pion production have very similar  $P_v$  distributions. We also find that the four-body  $\bar{p}p$  nonannihilation final-state events and the  $\pi^+p$  forward-hemisphere two-pion production events have similar  $P_v$  distributions. However, the distributions for annihilation and nonannihilation events are very different. We draw some conclusions about the production mechanisms involved. Section V summarizes our conclusions.

### II. DEFINITION OF $P_v$

In a previous publication<sup>1</sup> a kinematical variable  $R/R_{\max}$  was briefly described. In this paper we replace this notation with  $P_v \equiv R/R_{\max}$ .  $P_v$  is a peripherality variable which has the property that if  $P_v = 1$ , then all particles in the final state are collinear with the incoming beam, and if  $P_v = 0$ , then all final-state particles lie in a plane perpendicular to the incident beam. In the center-of-mass reference frame,  $P_v$  has a geometric interpretation in terms of the longitudinal momentum of all the final-state particles and the Van Hove longitudinal-phase-space analysis.<sup>2</sup> For a given final-state configuration, the longitudinal momenta of the particles have well-defined ratios with respect to each other, which can be expressed in terms of the Van Hove angle variables. These ratios are not unique to a given configuration; rather, there is an infinity of different configurations that have the same well-defined ratios. However, there is one configuration that is unique, that configuration in which all the particles in the final state are collinear with the incident beam direction. We will demonstrate later that this configuration can actually occur. In terms of the Van Hove analysis, this occurs when the event lies on the kinematical boundary and  $P_v = 1$ . If all the final-state particles lie in a plane perpendicular to the incident beam, then the longitudinal momentum of each particle is identically zero. In this

case, the event lies at the origin of the Van Hove plot and  $P_v = 0$ . Hence,  $P_v$  measures, in some sense, how collinear the event is with respect to the incident beam. We will give a quantitative statement of this in the following discussion.

As background, we will review some of the aspects of the Van Hove longitudinal-momentum analysis which are relevant here. Figure 1 contains the three-body Van Hove plot. In this plot, two quantities are defined:

$$\theta = \tan^{-1} \left( \frac{q_2 - q_3}{\sqrt{3} q_1} \right) + 90^\circ, \quad (1)$$

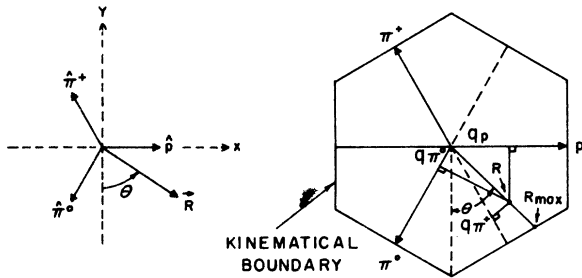
$$R = \left[ \frac{2}{3} (q_1^2 + q_2^2 + q_3^2) \right]^{1/2}, \quad (2)$$

where  $q_i$  = longitudinal momentum of the  $i$ th particle. The kinematical boundary is shown and  $R_{\max}$  is the intersection of the extension of the vector  $R$  (at fixed  $\theta$ ) with this boundary. We now define our peripherality variable:

$$P_v = \frac{R}{R_{\max}}. \quad (3)$$

One can calculate  $R_{\max}$  from energy conservation for the general  $n$ -body final state.<sup>3</sup> Let  $\vec{p}_i$ ,  $i = 1$  to  $n$ , be the three-momenta of the  $n$  particles of an  $n$ -body final state. If the  $p$ 's are measured in the center-of-mass frame of reference of the  $n$  particles, then

$$\sum_{i=1}^n \vec{p}_i = 0. \quad (4)$$



$$R = \left[ \frac{2}{3} (q_p^2 + q_{\pi^+}^2 + q_{\pi^0}^2) \right]^{1/2}$$

$$\theta = \tan^{-1} \left( \frac{q_{\pi^+} - q_{\pi^0}}{\sqrt{3} q_p} \right) + 90^\circ$$

FIG. 1. The three-body Van Hove longitudinal phase-space plot for  $\pi^+ p \rightarrow p \pi^+ \pi^0$ . The proton,  $\pi^+$ , and  $\pi^0$  unit vectors, defined as  $\hat{p}$ ,  $\hat{\pi}^+$  and  $\hat{\pi}^0$ , are at  $120^\circ$  with respect to each other. The simple kinematical boundary shown is calculated assuming that the rest masses are negligible compared with the center-of-mass energy. The polar coordinates,  $R$  and  $\theta$ , are defined in terms of the longitudinal momentum of the three final-state particles.

The  $n$  longitudinal momenta  $q_1, \dots, q_n$  are defined by

$$q_i = \hat{b} \cdot \vec{p}_i, \quad (5)$$

where  $\hat{b}$  is the unit vector in the direction of the incident beam particle in the center-of-mass frame of reference. Thus,

$$\sum_{i=1}^n q_i = 0. \quad (6)$$

Therefore, only  $n-1$  of the  $q$ 's are independent, and hence all  $n$   $q$ 's can be represented by  $n-1$  coordinates. Let  $\hat{\alpha}_i$  be a set of  $n$  unit vectors in  $(n-1)$ -dimensional space. Our aim is to arrange the angles between the  $n$  unit vectors so that for any  $n$ -body final state we can define a vector  $\vec{X}$  such that

$$\vec{X} \cdot \hat{\alpha}_i = q_i \quad (7)$$

and, conversely, any vector  $\vec{X}$  can represent the longitudinal momentum of the  $n$  particles in an  $n$ -body final state. From Eqs. (6) and (7) and for arbitrary  $\vec{X}$  the following equation holds:

$$\begin{aligned} \vec{X} \cdot \left( \sum_{i=1}^n \hat{\alpha}_i \right) &= \sum_{i=1}^n \vec{X} \cdot \hat{\alpha}_i \\ &= \sum_{i=1}^n q_i \\ &= 0. \end{aligned} \quad (8)$$

This proves that

$$\sum_{i=1}^n \hat{\alpha}_i = 0. \quad (9)$$

From this it follows that

$$\hat{\alpha}_i = - \sum_{j \neq i}^n \hat{\alpha}_j. \quad (10)$$

From symmetry, we will require that all the unit vectors make the same angle with each other. This implies that

$$\hat{\alpha}_i \cdot \hat{\alpha}_j = \cos \theta_{ij} = C \quad (i \neq j). \quad (11)$$

We will show that

$$C = -\frac{1}{n-1}. \quad (12)$$

From Eq. (10) and the fact that  $|\hat{\alpha}_i|^2 = 1$ , we have

$$\begin{aligned} \hat{\alpha}_i \cdot \hat{\alpha}_i &= 1 \\ &= \hat{\alpha}_i \cdot \left( - \sum_{j \neq i}^n \hat{\alpha}_j \right) \\ &= - \sum_{j \neq i}^n \hat{\alpha}_i \cdot \hat{\alpha}_j \\ &= -(n-1)C. \end{aligned} \quad (13)$$

This implies that

$$C = \hat{\alpha}_i \cdot \hat{\alpha}_j = -\frac{1}{n-1} = \cos \theta_{ij} \quad (i \neq j). \quad (14)$$

A set of  $n$  unit vectors in  $(n-1)$ -dimensional space satisfying Eqs. (9), (10), and (14) is

$$\begin{aligned} \alpha_i^j &= 0, \quad i < j \leq n-1, \\ \alpha_i^j &= \left[ \frac{n(n-j)}{(n-1)(n-j+1)} \right]^{1/2}, \quad i=j \leq n-1, \\ \alpha_i^j &= -\left[ \frac{n}{(n-1)(n-j+1)(n-j)} \right]^{1/2}, \quad j < i \leq n-1 \end{aligned} \quad (15)$$

with

$$\hat{\alpha}_n = -\sum_{i=1}^{n-1} \hat{\alpha}_i,$$

where  $\alpha_i^j$  is the  $j$ th component of the  $i$ th unit vector. From Eq. (7) we see that

$$\sum_{i=1}^n q_i^2 = \sum_{i=1}^n (\vec{X} \cdot \hat{\alpha}_i)^2. \quad (16)$$

Without loss of generality, for the purpose of calculating  $R = |\vec{X}|$ , we can assume  $\vec{X} = |\vec{X}| \hat{\alpha}_1 = R \hat{\alpha}_1$ . With this assumption Eq. (16) becomes

$$\begin{aligned} \sum_{i=1}^n q_i^2 &= \sum_{i=1}^n (R \hat{\alpha}_1 \cdot \hat{\alpha}_i)^2 \\ &= R^2 + R^2 \sum_{i=2}^n \left( \frac{-1}{n-1} \right)^2 \\ &= R^2 + R^2 (n-1) \frac{1}{(n-1)^2} \\ &= \frac{R^2 n}{(n-1)}, \end{aligned} \quad (17)$$

which implies that

$$R^2 = \frac{n-1}{n} \sum_{i=1}^n q_i^2. \quad (18)$$

The total energy  $E$  is given by

$$E = \sum_{i=1}^n [q_i^2 + (p_{ti})^2 + m_i^2]^{1/2}, \quad (19)$$

where, as above,  $q_i$  is the longitudinal momentum,  $m_i$  is the mass, and  $(p_{ti})^2$  is the square of the absolute value of the transverse momentum of the  $i$ th particle in the final state. The following inequality is useful here:

$$E = \sum_{i=1}^n [q_i^2 + (p_{ti})^2 + m_i^2]^{1/2} \geq \sum_{i=1}^n (q_i^2 + m_i^2)^{1/2}. \quad (20)$$

A scale factor  $w$  may be defined by the equation

$$\sum_{i=1}^n (w^2 q_i^2 + m_i^2)^{1/2} = E. \quad (21)$$

The inequality in Eq. (20) ensures the existence of a positive real value for  $w$ ,  $w \geq 1$ . In the extreme case where all  $q_i \equiv 0$ , then  $w$  is defined to be infinity.

As can be seen in Eq. (1) for the three-body final state, multiplying each  $q_i$  by fixed  $w$  does not change the value of  $\theta$ . Or, saying it in another way, multiplying each longitudinal momentum by a fixed  $w$  does not change the ratios of the longitudinal momenta. This comment is also true for the  $n$ -body final state. Since the Van Hove angular variables merely reflect longitudinal momentum orderings, multiplying each  $q_i$  by a constant leaves all the Van Hove angular variables invariant.<sup>3</sup> Geometrically, if you multiply each  $q_i$  by a scale factor, all Van Hove angles remain constant, but the radius changes. The events on the kinematical boundary satisfy Eq. (21) with  $w = 1$ .

Hence, given the value  $w$  which satisfied Eq. (21) for a fixed final state, then the  $(wq_i)$  define an event which is on the kinematic boundary of the Van Hove plot. Therefore,  $R_{\max}$  is given by

$$\begin{aligned} R_{\max} &= \left( \frac{n-1}{n} \sum_{i=1}^n w^2 q_i^2 \right)^{1/2} \\ &= w \left( \frac{n-1}{n} \sum_{i=1}^n q_i^2 \right)^{1/2} \\ &= wR. \end{aligned} \quad (22)$$

It therefore follows that

$$P_v = 1/w. \quad (23)$$

One can calculate  $P_v$  by solving Eq. (21) numerically. If  $P_v = 1$ , none of the particles in the final state have any transverse momentum and the event is completely collinear. If  $P_v = 0$ , then  $R = 0$  and from Eq. (18) each  $q_i$  must be identically zero. Thus, all particles have only transverse momenta, and the event lies in a plane perpendicular to the incident beam. An important property of this variable is that it characterizes the whole event and is not representative of a class of particles in the final state.

$P_v$  has an interesting high-energy limiting behavior, namely,

$$P_v \underset{E \rightarrow \infty}{\sim} 2 \sum_{i=1}^n |X_i|, \quad (24)$$

where  $X_i$  is the Feynman variable<sup>4</sup> for the  $i$ th particle (i.e.,  $X_i = q_i / 2\sqrt{s} = q_i / 2E$ ). This can be seen by solving Eq. (21) for the case of very large  $E$ .

From Eq. (21) we have

$$\sum_{i=1}^n \left( \frac{w^2 q_i^2}{E^2} + \frac{m_i^2}{E^2} \right)^{1/2} = 1. \quad (25)$$

If  $E \gg m_i$ , then even for  $q_i \sim 0$  we have

$$\left( \frac{w^2 q_i^2}{E^2} + \frac{m_i^2}{E^2} \right)^{1/2} \cong \frac{w |q_i|}{E} + m_i O(m_i/E) \quad (26)$$

and Eq. (25) becomes

$$\sum_{i=1}^n w \frac{|q_i|}{E} + \sum_{i=1}^n m_i O(m_i/E) = 1. \quad (27)$$

For fixed  $n$

$$\sum_{i=1}^n m_i O(m_i/E) \cong 0$$

and Eq. (27) reduces to

$$1 = \sum_i w \frac{|q_i|}{E} = w \sum_i \frac{|q_i|}{E}, \quad (28)$$

$$\frac{1}{w} = P_v \cong \sum_{i=1}^n \frac{|q_i|}{E} = 2 \sum_{i=1}^n |X_i|.$$

Hence, in the limit of large total energy,  $P_v$  is twice the sum of all the absolute values of the Feynman variables for that final state. Therefore, any exclusive process that has a limiting distribution in terms of the Feynman variable will also have a limiting distribution in  $P_v$ .

### III. PROPERTIES OF $P_v$

As stated in Sec. II, any distribution that has a limiting distribution in the Feynman  $X$  variables as the final-state energy approaches infinity will have a limiting distribution in  $P_v$ . An obvious example of this is Lorentz-invariant phase space. When the total energy in the center-of-mass sys-

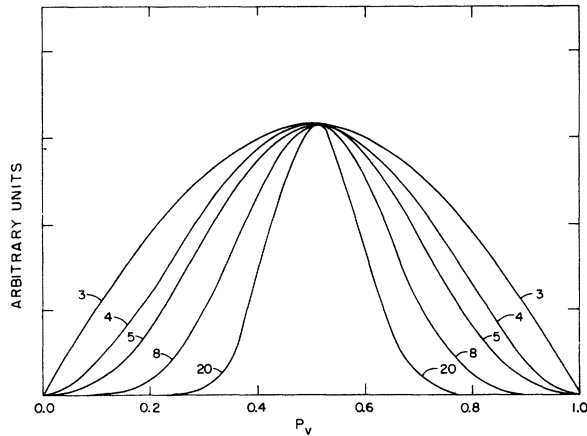


FIG. 2. Monte Carlo  $P_v$  distributions for Lorentz-invariant phase space for  $n$ -body final-state configurations. The reaction assumed was  $\pi^+ + p \rightarrow p + (n-1)\pi$ ,  $n=3, 4, 5, 8, 20$ , at an incident pion momentum of 100 GeV/c. The shapes shown do not change significantly for incident momenta down to 5 GeV/c.

tem becomes large compared to the sum of the masses in the final state, the distribution of the  $X$  variable becomes energy-independent and, hence, so does the distribution of  $P_v$ .

Figure 2 shows the  $P_v$  distributions from Monte Carlo calculations of Lorentz-invariant phase space for various  $n$ -body final states of the reaction  $\pi^+ p \rightarrow p + (n-1)\pi$  at 100 GeV incident  $\pi^+$  momentum. The most notable feature of these curves is that, as  $n$  increases, the peaking near  $P_v=0.5$  becomes more pronounced and the regions around  $P_v=0$  and  $P_v=1$  become more depleted. These curves are slightly asymmetric, tending to shift towards  $P_v=1$ . This tendency increases with increasing  $n$  and decreasing incident momentum. However, there is no significant change in shape even for momentum as low as 5 GeV/c.

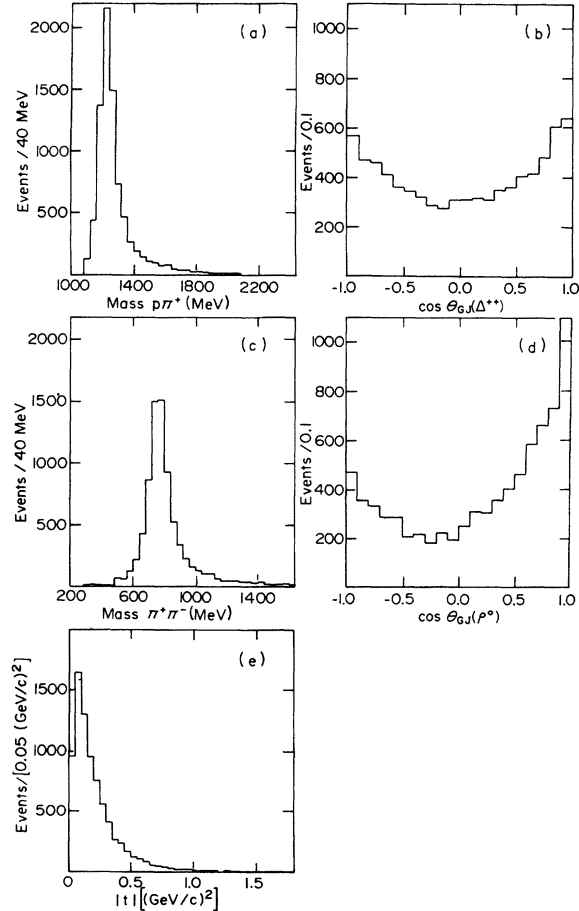


FIG. 3. Monte Carlo distributions for the reaction  $\pi^+ p \rightarrow \Delta^{++} \rho^0$  for incident pion momentum of 10 GeV/c: (a) the assumed  $\Delta^{++}$  invariant mass; (b) the  $\Delta^{++}$  Gottfried-Jackson angle; (c) the assumed  $\rho^0$  invariant mass; (d) the  $\rho^0$  Gottfried-Jackson angle; (e) the production  $t$  distribution. The Treiman-Yang distribution for both the  $\Delta^{++}$  and  $\rho^0$  was assumed to be isotropic.

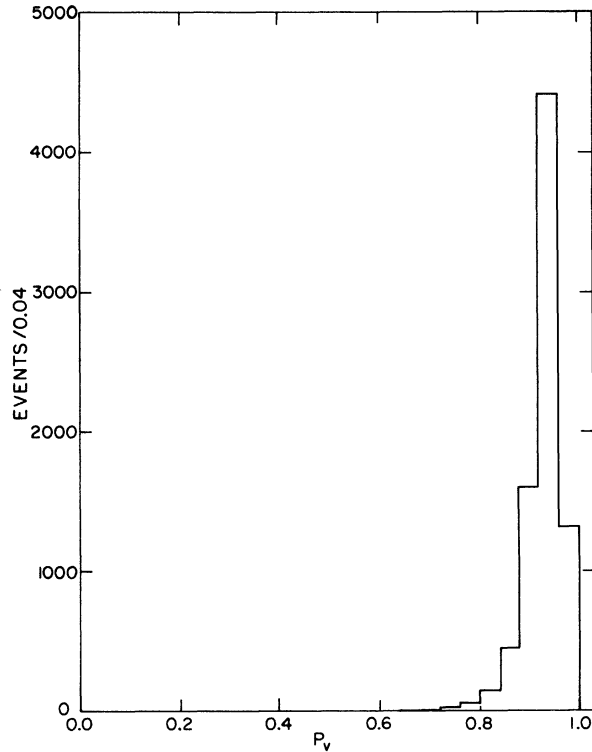


FIG. 4. The  $P_v$  distribution for the  $\pi^+p \rightarrow \Delta^{++}\rho^0$  Monte Carlo data shown in Fig. 3. This distribution peaks near  $P_v=1$ , which is in sharp contrast with the Lorentz-invariant phase-space distribution shown in Fig. 2.

This behavior can be contrasted with that typical of resonance production in the final state. For example, the  $P_v$  distribution may be calculated by Monte Carlo methods for the four-body reaction



at 10 GeV/c incident pion momentum. Figure 3 gives the invariant mass, Gottfried-Jackson angle, and  $t$  distributions used for the  $\Delta^{++}$  and  $\rho^0$  in this calculation. Figure 4 gives the resulting  $P_v$  distribution for reaction (29). Note the peaking near  $P_v=1.0$ .

Although  $P_v$  is related to the peripherality of the whole event, it is not the same as the four-momentum transfer  $t$ . To demonstrate this, we have taken a cut on our Monte Carlo sample considering only those events which have a  $P_v > 0.92$ . This includes 70% of the original sample. In Fig. 5 we plot the  $t'$  ( $t' \equiv t - t_{\min}$ ) distribution for both the original sample and for our reduced sample with  $P_v > 0.92$ . We also indicate on the figure the value of  $t'$  which divides the data such that 70% of the original sample has a  $t'$  less than this value. This figure demonstrates that a cut on  $P_v$  is not the same as a cut on  $t'$  (or  $t$ ).

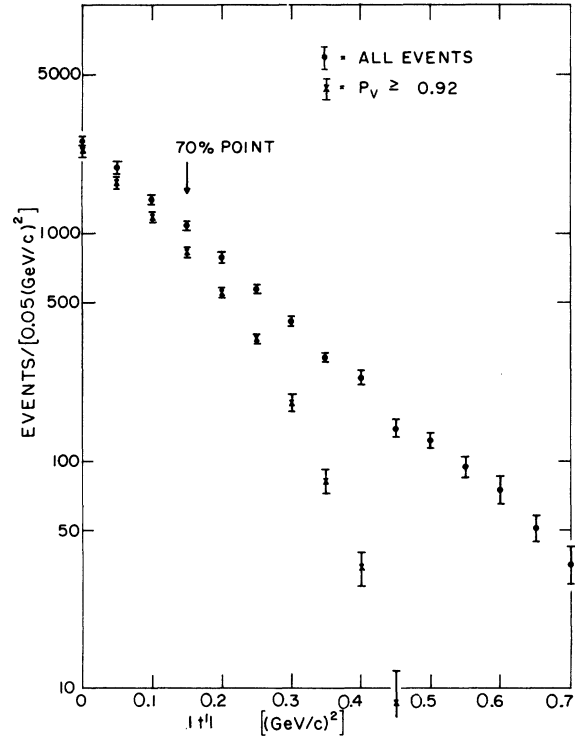


FIG. 5. The  $t'$  ( $t' = t - t_{\min}$ ) distribution for the  $\pi^+p \rightarrow \Delta^{++}\rho^0$  Monte Carlo data for all values of  $P_v$ , compared with the  $t'$  distribution for those events for which  $P_v \geq 0.92$ . The latter sample contains 70% of the events. A sample obtained by a cut on  $t'$  would require  $|t'| \leq 0.15$  if it were to contain the same number of events. This comparison demonstrates that a cut on  $P_v$  is not identical to a cut on  $t'$ .

As an illustrative example to demonstrate the utility of  $P_v$ , we have combined 20% of four-body Lorentz-invariant phase space with 80% of reaction (29). We show in Fig. 6 the  $p\pi^+$  and  $\pi^+\pi^-$  invariant-mass distributions for this mixture. As expected, these histograms show clear  $\Delta^{++}$  and  $\rho^0$  signals riding on top of a 20% background. The phase-space events are plotted choosing that  $p\pi^+$  combination which is closest to the  $\Delta^{++}$  mass as the  $\Delta^{++}$ . Figure 7 gives the  $P_v$  distribution for the mixture, and it is seen that a cut at about  $P_v = 0.8$  would eliminate almost all the phase-space events and very few of the events of reaction (29). Figure 8, which displays the distributions corresponding to events for which  $P_v \geq 0.8$ , is essentially indistinguishable from Fig. 3. In particular, the  $t$  distributions displayed in Figs. 3(e) and 8(e) are essentially identical. Hence, in this particular situation, a cut on  $P_v$  would be very useful in eliminating Lorentz-invariant phase-space events from the sample.

Of particular interest is the possibility of using  $P_v$  as a variable in order to detect phase-space-

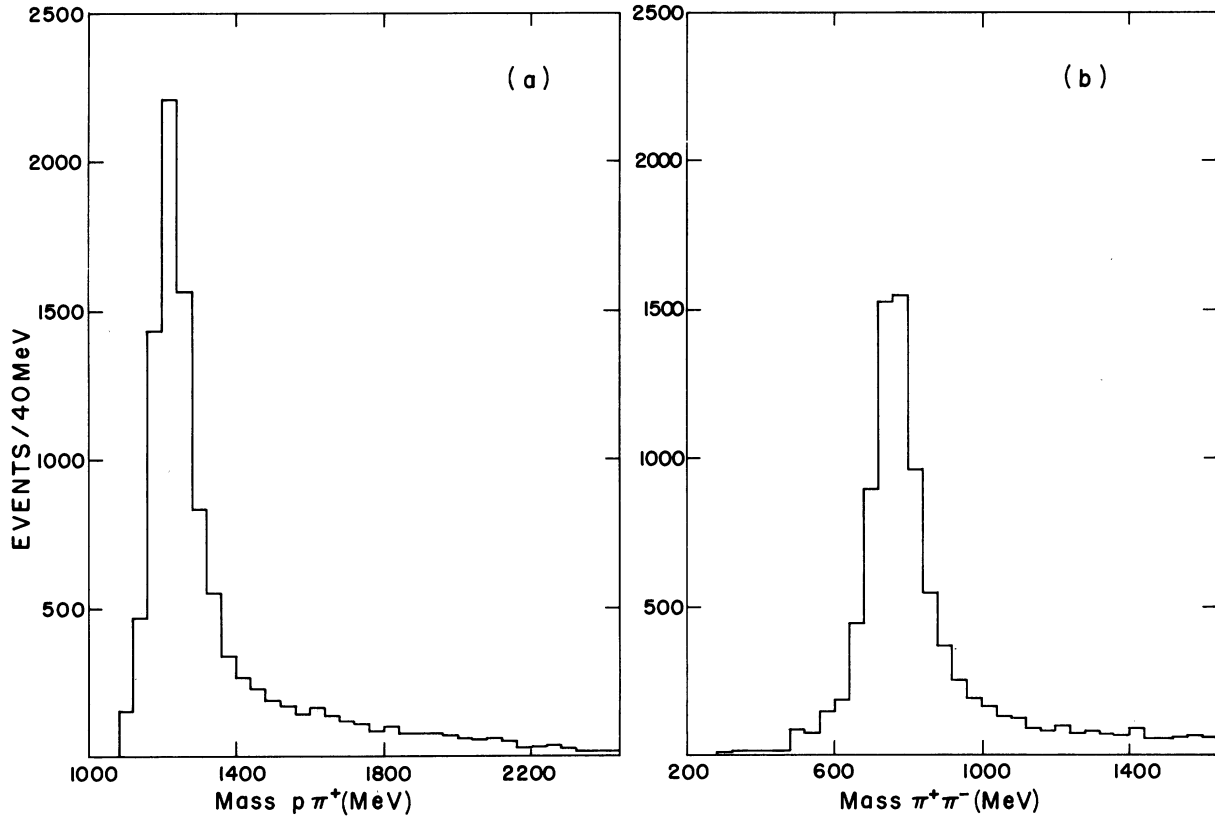


FIG. 6. The  $p\pi^+$  and  $\pi^+\pi^-$  invariant mass distributions resulting from a mixture of 20% Lorentz-invariant phase space and 80%  $\Delta^{++}\rho^0$  production. The  $\Delta^{++}\rho^0$  Monte Carlo sample is characterized by the distributions shown in Fig. 3. The phase-space events are plotted by choosing the  $p\pi^+$  combination with invariant mass closest to the  $\Delta^{++}$ .

like processes in multibody ( $n \geq 10$ ) final states at high energies. The distribution of  $P_v$  for large  $n$  shown in Fig. 2 indicates that this type of process should be distinguishable from peripheral-type mechanisms, such as quasiresonance production or diffraction dissociation.

#### IV. APPLICATION

Since  $P_v$  is a variable that characterizes the whole event, it is useful to try and consider what processes would affect its distribution. In the framework of particle-exchange models, there are really just two classes of exchange mechanisms—one is meson exchange and the other is baryon exchange. Hence, it would be useful to compare the  $P_v$  distribution in cases where only the exchange mechanism is a common property.  $\bar{p}p$  annihilation processes are examples of pure baryon exchange. Backward production of mesons by  $\pi p$  interactions (mesons produced in those events where the nucleon changes direction in the center-of-mass system) is also thought to be dominated by baryon exchange. Hence, one could compare the  $P_v$  dis-

tributions of  $\bar{p}p$  annihilation events with backward meson production by pions. One could also compare meson production by  $\bar{p}p$  nonannihilation interactions with forward meson production by  $\pi p$  interactions (mesons produced in those events where the nucleon does not change direction in the center-of-mass system), since both processes are dominated by meson exchanges.

Previous authors have studied the transverse-momentum distributions of particles in  $\bar{p}p$  annihilation and nonannihilation channels.<sup>5-12</sup> Studies have also been made comparing two-body annihilation processes to backward elastic scattering.<sup>13,14</sup> These comparisons are based on baryon-exchange concepts. A study of  $K^-p$  interactions which attempts to isolate baryon-exchange mechanisms has also been reported.<sup>15,16</sup> Other authors have studied the backward peaks in resonance production in  $\pi p$  interactions.<sup>17</sup> In these resonant studies, it was found that the angular distributions were not as sharply peaked backward as they are peaked forward. This difference was interpreted as evidence for baryon exchange in the backward direction for these resonant processes.

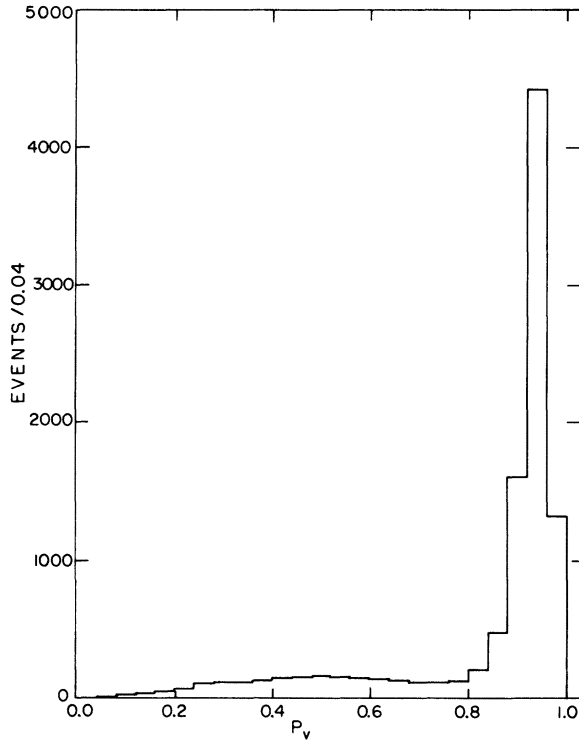


FIG. 7. The  $P_v$  distribution for the Monte Carlo events shown in Fig. 6.

Since we have data on both  $\pi p$  and  $\bar{p}p$  interactions, we report here a study of four-body final states produced by incident 3.9-GeV/c and 5.7-GeV/c  $\pi^+$  on hydrogen and four-body annihilation and nonannihilation final states produced by incident 4.4-GeV/c and 5.1-GeV/c  $\bar{p}$  on hydrogen. The data were taken from exposures in the ANL 30-in. hydrogen bubble chamber. The sample is a subset of over 200 000 events measured on PEPR (Precision Encoding and Pattern Recognition).

We have analyzed these data, both with respect to the conventional transverse-momentum distributions and with respect to  $P_v$ . We consider the conventional method of describing the data first.

Consider the reaction  $\pi^+p \rightarrow p\pi^+\pi^+\pi^-$ . We define a forward event as one in which the proton does not change its direction and goes into its forward hemisphere in the center-of-mass system. We define a backward event as one in which the proton reverses its direction in the center-of-mass system and goes into its backward hemisphere. In Fig. 9 we plot the  $P_\perp$  and  $(P_\perp)^2$  distributions for incident pion momentum of 3.9 GeV/c. As can be seen, the distributions for pions and protons from forward events are slightly different, with the protons having a somewhat broader distribution. The pions from backward events have a distribution not too different from the protons from for-

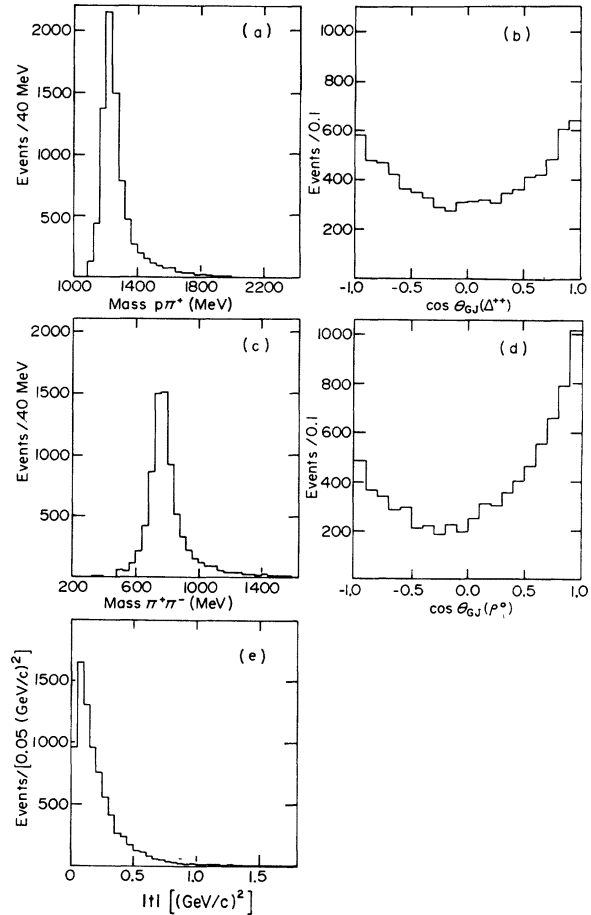


FIG. 8. Distributions for the Monte Carlo events shown in Fig. 6 for which  $P_v \geq 0.8$  (see Fig. 7): (a) the  $\Delta^{++}$  invariant mass; (b) the  $\Delta^{++}$  Gottfried-Jackson angle; (c) the  $\rho^0$  invariant mass; (d) the  $\rho^0$  Gottfried-Jackson angle; (e) the  $t$  distribution.

ward events, while the protons from backward events have the broadest distribution. Similar comments can be made about the 5.7-GeV/c data (Fig. 10).

In comparing backward and forward events, the obvious question that arises is: Which are the important distributions? Does one consider only the pions or does one concentrate on the protons, or should one study some combination of distributions?

In Figs. 11 and 12 we display the  $P_\perp$  and  $(P_\perp)^2$  distributions obtained from the data for the reactions

$$\bar{p} + p \rightarrow \bar{p} + p + \pi^+ + \pi^-, \quad (30)$$

$$\bar{p} + p \rightarrow \pi^+ + \pi^+ + \pi^- + \pi^- \quad (31)$$

at 4.4 and 5.1 GeV/c incident  $\bar{p}$  momentum, respectively. For reaction (30) distributions for both pions and baryons are given. The distribu-

tions for the baryons are slightly broader than those for the pions. The distributions for the pions for reaction (31) are, however, even broader.

If we wish to compare the meson-induced final

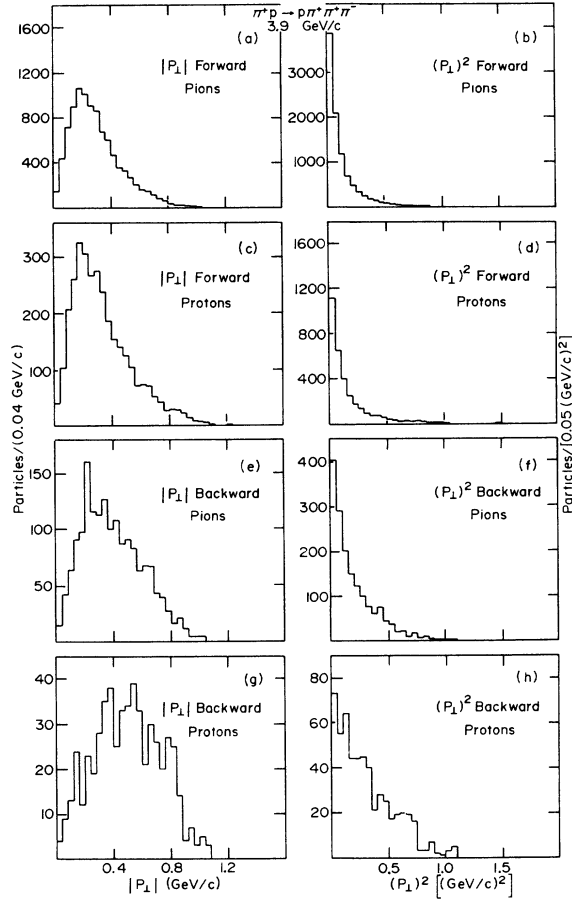


FIG. 9. The  $P_{\perp}$  and  $(P_{\perp})^2$  distributions for the final-state particles in the reaction  $\pi^+p \rightarrow p\pi^+\pi^+\pi^-$  at 3.9 GeV/c: (a) the transverse-momentum distribution of the pions from the forward-hemisphere events (a forward-hemisphere event is one in which the outgoing proton is emitted in the forward hemisphere in the center-of-mass system with respect to the direction of the incoming proton); (b) the transverse-momentum-squared distribution of pions from forward-hemisphere events; (c) the transverse-momentum distribution of protons from forward-hemisphere events; (d) the transverse-momentum-squared distribution of protons from forward-hemisphere events; (e) the transverse-momentum distribution of pions from backward-hemisphere events (a backward-hemisphere event is one in which the outgoing proton is emitted in the backward hemisphere in the center-of-mass system with respect to the direction of the incoming proton); (f) the transverse-momentum-squared distribution of pions from backward-hemisphere events; (g) the transverse-momentum distribution of protons from backward-hemisphere events; (h) the transverse-momentum-squared distribution of protons from backward-hemisphere events.

states with the antiproton-induced final states, we have to make some arbitrary choices as to which distributions to compare. If we have production of a particular resonance, it makes sense, of course, to look at the peaking of the angular distribution. However, if, as in this case, we are examining all the final-state reactions at once, the concept of an angular distribution is difficult

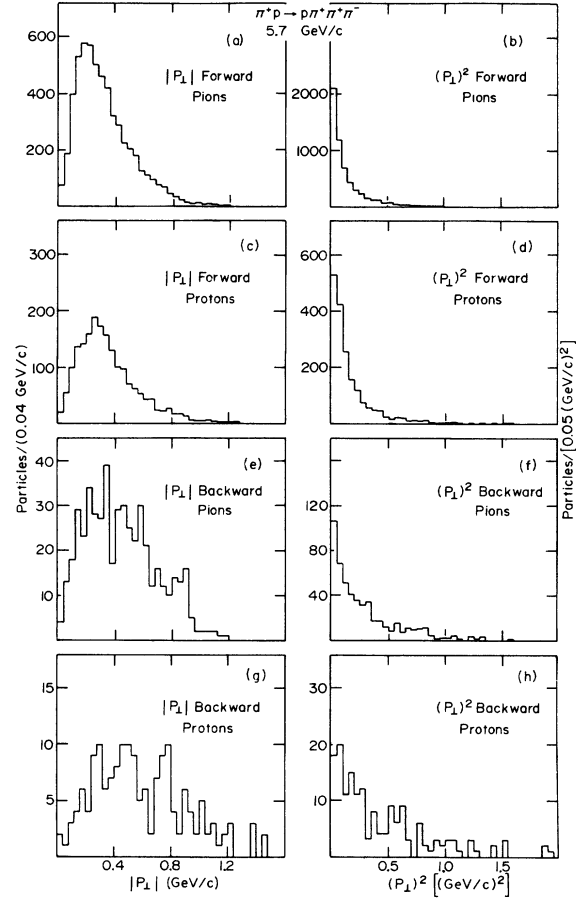


FIG. 10. The  $P_{\perp}$  and  $(P_{\perp})^2$  distributions for the final-state particles in the reaction  $\pi^+p \rightarrow p\pi^+\pi^+\pi^-$  at 5.7 GeV/c: (a) the transverse-momentum distribution of the pions from forward-hemisphere events (see Fig. 9 or text for the definition of forward-hemisphere event); (b) the transverse-momentum-squared distribution of pions from forward-hemisphere events; (c) the transverse-momentum distribution of protons from forward-hemisphere events; (d) the transverse-momentum-squared distribution of protons from forward-hemisphere events; (e) the transverse-momentum distribution of pions from backward-hemisphere events (see Fig. 9 or text for definition of backward-hemisphere events); (f) the transverse-momentum-squared distribution of pions from backward-hemisphere events; (g) the transverse-momentum distribution of protons from backward-hemisphere events; (h) the transverse-momentum-squared distribution of protons from backward-hemisphere events.



to define.

If we analyze the complete final state in terms of the variable  $P_v$ , it is not necessary to make an arbitrary choice. The virtue of the variable  $P_v$  is that it characterizes the final state of an event rather than that of an individual final-state particle. Figure 13 demonstrates the utility of this characteristic of  $P_v$ . Figures 13(a) and 13(b) compare the forward-hemisphere events induced by 3.9-GeV/c  $\pi^+$  mesons on protons with the nonannihilation 4.4-GeV/c  $\bar{p}p$  data. The center-of-mass incident momentum for the  $\pi^+p$  data is 1.28 GeV/c, which is almost equal to the 1.29-GeV/c center-of-mass incident momentum for the  $\bar{p}p$  data. These two distributions are almost identical.

Figures 13(e) and 13(f) compare the forward-hemisphere events induced by incident 5.7-GeV/c  $\pi^+$  mesons with the nonannihilation 5.1-GeV/c  $\bar{p}p$  data. The center-of-mass incident momentum for the 5.7-GeV/c  $\pi^+$  data is 1.58 GeV/c and that for the 5.1-GeV/c  $\bar{p}p$  data is 1.4 GeV/c. Again, the

two momenta are similar and so are the two distributions. It is seen that for the forward-hemisphere  $\pi^+p$  data and for the nonannihilation data, the higher the incident momentum in the center-of-mass system, the more the distribution is peaked near  $P_v = 1$ .

If we now look at Fig. 13(c), which gives the  $P_v$  distribution for the backward-hemisphere events induced by 3.9-GeV/c  $\pi^+$  mesons on protons, we find a strikingly different distribution compared with that for the forward-hemisphere events. In Fig. 13(d) we plot the  $P_v$  distribution for the annihilation events for the 4.4-GeV/c  $\bar{p}p$  data. The similarity of the  $P_v$  distributions between the backward-hemisphere events and the annihilation events is quite obvious. The same similarities exist for Figs. 13(g) and 13(h), which show the 5.7-GeV/c  $\pi^+p$  data and the 5.1-GeV/c  $\bar{p}p$  data, respectively.

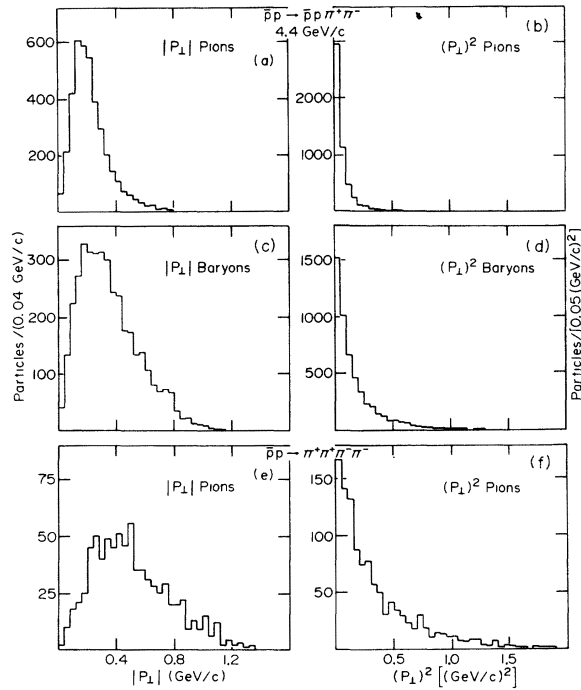


FIG. 11. The  $P_L$  and  $(P_L)^2$  distributions for the final-state particles in the reactions (A)  $\bar{p}p \rightarrow \bar{p}p\pi^+\pi^-$  and (B)  $\bar{p}p \rightarrow \pi^+\pi^+\pi^-\pi^-$  at 4.4 GeV/c: (a) the transverse-momentum distribution of the pions for reaction (A); (b) transverse-momentum-squared distribution of the pions for reaction (A); (c) the transverse-momentum distribution of the baryons for reaction (A); (d) the transverse-momentum-squared distribution of the baryons for reaction (A); (e) the transverse-momentum distribution of the pions for reaction (B); (f) the transverse-momentum-squared distribution of the pions for reaction (B).

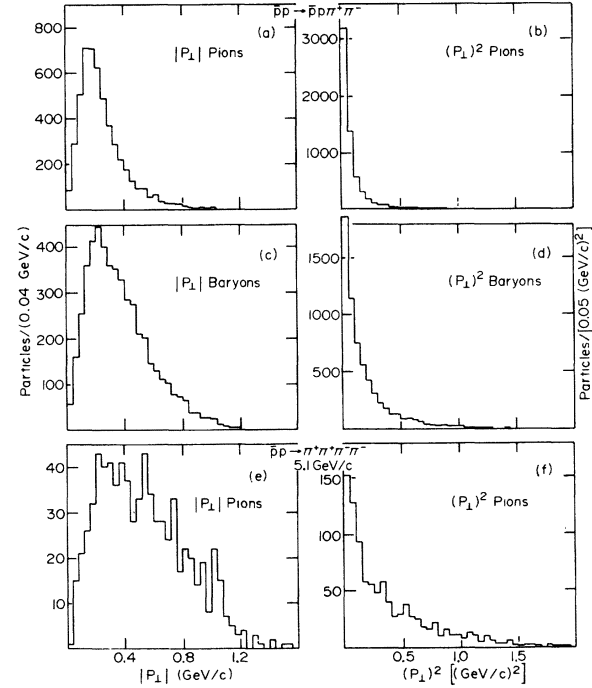


FIG. 12. The  $P_L$  and  $(P_L)^2$  distributions for the final-state particles in the reactions (A)  $\bar{p}p \rightarrow \bar{p}p\pi^+\pi^-$  and (B)  $\bar{p}p \rightarrow \pi^+\pi^+\pi^-\pi^-$  at 5.1 GeV/c: (a) the transverse-momentum distribution of the pions for reaction (A); (b) the transverse-momentum-squared distribution of the pions for reaction (A); (c) the transverse-momentum distribution of the baryons for reaction (A); (d) the transverse-momentum-squared distribution of the baryons for reaction (A); (e) the transverse-momentum distribution of the pions for reaction (B); (f) the transverse-momentum-squared distribution of the pions for reaction (B).

We believe that the similarity between the annihilation channel and the  $\pi^+p$  channel with backward hemisphere data is due to the fact that both channels are dominated by baryon exchange. Furthermore, we believe that the similarity between the nonannihilation  $\bar{p}p$  channel and the  $\pi^+p$  channel with forward-hemisphere data is due to the fact that these channels are dominated by meson exchange. Note that we have not had to isolate resonant reactions to come to these conclusions.

If the above explanation does indeed have validity, we make the following predictions:

Final states dominated by meson exchanges will have  $P_v$  distributions similar to those in Figs. 13(a), 13(b), 13(e), and 13(f). Reactions with the same number of particles and similar incident momentum in the center-of-mass system will have similar  $P_v$  distributions. The higher this momentum, the more the  $P_v$  distribution will peak toward  $P_v = 1$ .

Final states dominated by baryon exchanges will have  $P_v$  distributions similar to those in Figs. 13(c), 13(d), 13(g), and 13(h). Reactions with the same number of particles and similar momentum in the center-of-mass system will have similar  $P_v$  distributions. The higher the momentum, the more the  $P_v$  distribution will shift towards  $P_v = 1$ .

An additional test of the above ideas can be made by studying the reaction  $p + n \rightarrow p + n + \pi^+ + \pi^-$ . The backward hemisphere in this reaction (those events where the proton and the neutron both reverse direction in the center-of-mass system) is a region of meson exchange rather than a region of baryon exchange. Hence, for this reaction, if you plot  $P_v$  for the events in which the baryons both reverse direction, the distribution should be the same as the  $P_v$  distribution for the  $\pi^+p$  events with forward-hemisphere data. These distributions should be similar to those of Figs. 13(a), 13(b), 13(e), and 13(f). We also predict that the  $P_v$  distribution for events where both nucleons are in the forward hemisphere will be the same as when both nucleons are in the backward hemisphere (baryon exchange). These distributions should be similar to those of Figs. 13(c), 13(d), 13(g), and 13(h).

## V. CONCLUSIONS

We have defined a variable  $P_v$  which is characteristic of the complete multibody final state. This variable indicates the peripherality of the event and ranges in value between 0 and 1. When  $P_v = 0$ , all the particles of the final state are in a plane perpendicular to the incident direction. When  $P_v = 1$ , all particles are collinear with the incident direction. We also describe the relation

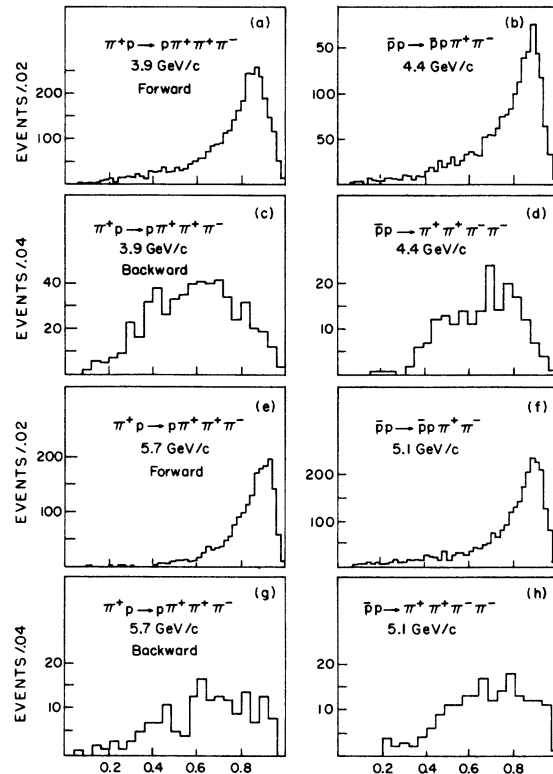


FIG. 13.  $P_v$  distributions for  $\pi^+$  and  $\bar{p}$  induced four-body final states: (a) the  $P_v$  distribution for forward events from  $\pi^+p \rightarrow p\pi^+\pi^+\pi^-$  at 3.9 GeV/c (see Fig. 9 or text for definition of forward events); (b) the  $P_v$  distribution for  $\bar{p}p \rightarrow \bar{p}p\pi^+\pi^-$  events at 4.4 GeV/c; (c) the  $P_v$  distribution for backward events from  $\pi^+p \rightarrow p\pi^+\pi^+\pi^-$  at 3.9 GeV/c (see Fig. 9 or text for the definition of backward events); (d) the  $P_v$  distribution for  $\bar{p}p \rightarrow \pi^+\pi^+\pi^-\pi^-$  events at 4.4 GeV/c; (e) the  $P_v$  distribution for forward events from  $\pi^+p \rightarrow p\pi^+\pi^+\pi^-$  at 5.7 GeV/c; (f) the  $P_v$  distribution for  $\bar{p}p \rightarrow \bar{p}p\pi^+\pi^-$  events at 5.1 GeV/c; (g) the  $P_v$  distribution for backward events from  $\pi^+p \rightarrow p\pi^+\pi^+\pi^-$  at 5.7 GeV/c; (h) the  $P_v$  distribution for  $\bar{p}p \rightarrow \pi^+\pi^+\pi^-\pi^-$  events at 5.1 GeV/c.

between  $P_v$  and the Feynman variables  $X_i$  in the limit of large energy. We have calculated the  $P_v$  distribution for the assumption that the final state is dominated by Lorentz-invariant phase space. We have also examined the behavior of the  $P_v$  distribution, assuming a resonant final state and a mixture of resonant final state with Lorentz-invariant phase space. We conclude that  $P_v$  is a useful variable to consider when trying to eliminate Lorentz-invariant phase space from a sample containing a quasi-two-body process. We also point out that the study of a  $P_v$  distribution could be very useful in detecting phase-space-like processes at high energy and large final-state multiplicities ( $n \geq 10$ ).

We have applied this variable to a study of  $\bar{p}p$  and  $\pi^+p$  four-body final states. We have presented evidence for kinematic similarities between the four-body annihilation channel in  $\bar{p}p$  interactions and four-body  $\pi^+p$  backward-hemisphere events at the same center-of-mass incoming momentum. A similarity exists for the  $\bar{p}p$  nonannihilation channels and  $\pi^+p$  forward-hemisphere events. However, the annihilation and nonannihilation channels are strikingly different when examined in terms of  $P_v$ , as are the backward and forward hemispheres in the pion-induced four-body final state. We believe these phenomena can be understood in terms of

the difference between baryon- and meson-exchange processes. We have proposed an experimental test of this hypothesis.

#### ACKNOWLEDGMENTS

We wish to thank the operating crew of the ANL 30-in. chamber who made this experiment possible. We are indebted to our scanning, measuring, and PEPR operators. We are also indebted to L. Van Hove, who suggested that we look into this phenomenon and proposed that baryon and meson exchanges may play an important role.

\*Work supported in part through funds provided by the U. S. Atomic Energy Commission under Contract No. AT(11-1) 3069 and the National Science Foundation under University Science Development Grant GU-2655.

†Permanent address: The Weizmann Institute of Science, Israel.

‡A. P. Sloane Foundation Research Fellow.

<sup>1</sup>J. E. Brau *et al.*, Phys. Rev. Lett. **27**, 1481 (1971).

<sup>2</sup>L. Van Hove, Phys. Lett. **28B**, 429 (1969); Nucl. Phys. **B9**, 331 (1969).

<sup>3</sup>Complete details are available in F. T. Dao, M. F. Hodous, I. A. Pless, and R. A. Singer, MIT PEPR Programming Note—Physics 101, 1971 (unpublished).

<sup>4</sup>R. P. Feynman, Phys. Rev. Lett. **23**, 1415 (1969).

<sup>5</sup>K. Böckmann *et al.*, Nuovo Cimento **42A**, 954 (1966).

<sup>6</sup>A. Friedman *et al.*, Phys. Rev. **167**, 1268 (1968).

<sup>7</sup>A. Friedman *et al.*, Phys. Rev. **176**, 1595 (1968).

<sup>8</sup>I. Bar-Nir *et al.*, Nucl. Phys. **B20**, 45 (1970).

<sup>9</sup>G. Alexander *et al.*, Nucl. Phys. **B23**, 557 (1970).

<sup>10</sup>G. Alexander *et al.*, Nucl. Phys. **B35**, 45 (1971).

<sup>11</sup>S. Humble *et al.*, Nucl. Phys. **B56**, 61 (1973).

<sup>12</sup>P. S. Gregory *et al.*, Phys. Lett. **43B**, 228 (1973).

<sup>13</sup>A. Białas and O. Czyżewski, Phys. Lett. **13**, 337 (1964).

<sup>14</sup>B. C. Barish *et al.*, Phys. Rev. Lett. **23**, 607 (1969).

<sup>15</sup>J. R. Fry *et al.*, Phys. Lett. **43B**, 146 (1973).

<sup>16</sup>J. R. Fry *et al.*, Phys. Lett. **41B**, 539 (1972).

<sup>17</sup>D. R. O. Morrison, in *High Energy Physics*, proceedings of the Fifteenth International Conference on High Energy Physics, Kiev, 1970, edited by V. Shelest (Naukova Dumka, Kiev, U.S.S.R., 1972).